

Article

Versatile Polyoxometalates of Different Structural Dimensionalities for Liquid Phase Catalytic Oxidation

Patrícia Neves ¹, Guilherme Simões ¹, Bogna D. Napruszewska ², Katarzyna Pamin ², Paweł Serda ³, Wiesław Łasocho ^{2,3,*} and Anabela A. Valente ^{1,*}

¹ Department of Chemistry, CICECO-Aveiro Institute of Materials, University of Aveiro, 3810-193 Aveiro, Portugal; pneves@ua.pt (P.N.); gui.simoes@ua.pt (G.S.)

² Jerzy Haber Institute of Catalysis and Surface Chemistry, Polish Academy of Sciences, Niezapominajek 8, 30-239 Kraków, Poland; ncnaprus@cyf-kr.edu.pl (B.D.N.); ncpamin@cyf-kr.edu.pl (K.P.)

³ Faculty of Chemistry, Jagiellonian University, Gronostajowa 2, 30-387 Kraków, Poland; serda@chemia.uj.edu.pl

* Correspondence: lasocha@chemia.uj.edu.pl (W.Ł.); atav@ua.pt (A.A.V.)

Abstract: Ionic polymolybdate compounds (IPOM) possessing the anions $[\text{Mo}_8\text{O}_{26}]^{4-}$ and $[\text{Mo}_3\text{O}_{10}]^{2-}$, and cyclohexylammonium (Cy6N) or anilinium (Anil) as organic cations, namely cyclohexylammonium β -octamolybdate dihydrate (1), cyclohexylammonium trimolybdate hydrate (2), anilinium β -octamolybdate dihydrate (3), anilinium trimolybdate tetrahydrate (4) and anilinium trimolybdate dihydrate (5), were synthesized via simple, eco-friendly one-pot routes. New crystal structures of 1, 2 and 5 were discovered. IPOM compounds with different structural dimensionality, density and ratio of the number of terminal oxo groups/molybdenum atoms ($n(\text{oxo})/\text{Mo}$) were developed. The IPOM compounds promoted the epoxidation of biobased olefins such as the fatty acid methyl esters methyl oleate and methyl linoleate with *tert*-butylhydroperoxide as oxidant, leading to conversions of at least 81% at 4 h, 70 °C and the corresponding epoxides. The reaction scope of applications for the IPOM catalysts covered cyclooctane oxidation.

Keywords: ionic; polymolybdate; epoxidation; fatty acid methyl esters; anilinium; cyclohexylammonium



Citation: Neves, P.; Simões, G.; Napruszewska, B.D.; Pamin, K.; Serda, P.; Łasocho, W.; Valente, A.A. Versatile Polyoxometalates of Different Structural Dimensionalities for Liquid Phase Catalytic Oxidation. *Catalysts* **2024**, *14*, 251. <https://doi.org/10.3390/catal14040251>

Academic Editors: Leonarda Liotta, Narendra Kumar, Konstantin Ivanov Hadjiivanov and Vincenzo Vaiano

Received: 5 January 2024

Revised: 15 March 2024

Accepted: 29 March 2024

Published: 10 April 2024



Copyright: © 2024 by the authors. Licensee MDPI, Basel, Switzerland. This article is an open access article distributed under the terms and conditions of the Creative Commons Attribution (CC BY) license (<https://creativecommons.org/licenses/by/4.0/>).

1. Introduction

In the transition to a bio-based economy, the epoxidation of olefins such as fatty acid methyl esters (FAMES) has attracted much attention because the epoxidized FAMES (EFAMES) have broad application profiles, e.g., for plasticizers, lubricants, polyurethanes, painting, coatings and adhesives, and improving the oxidation stability of biodiesel [1–6].

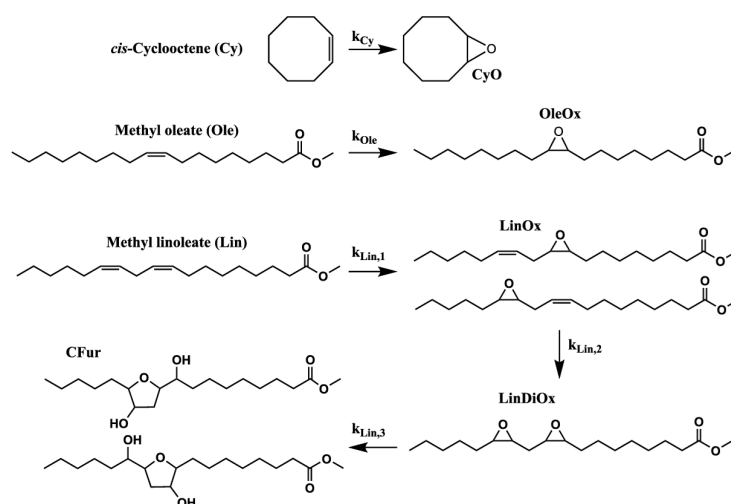
Moreover, EFAMES can be sustainably produced from waste and non-edible sources such as waste cooking oil and agricultural or industrial residues [7]. For example, crude tall oil is a by-product of the wood pulp industry with an average production of 30–50 kg per 1000 kg of processed wood. This oil contains *ca.* 30–50 wt.% of free fatty acids, which are mainly oleic acid and linoleic acid, and has high iodine value, i.e., many $\text{C}=\text{C}$ double bonds for epoxidation. Prominent players in the EFAMES market include DOW Chemical Company and KH Chemicals [8]. The industrial production of epoxidized vegetable oils based on the Prilezhaev peracid process involves percarboxylic acids, e.g., peracetic acid or performic acid, which may be formed via the reaction of the corresponding carboxylic acid with hydrogen peroxide [2,9–11]. These routes suffer from several drawbacks such as low epoxide selectivity, significant waste generation, safety, and corrosion issues associated with the strongly acidic media. This has led to research efforts in the fields of catalysis to develop efficient and less-hazardous epoxidation processes.

Molybdenum-based homogeneous catalysts reached industrial implementation in the 20th century for large-scale liquid phase epoxidation using *tert*-butylhydroperoxide (TBHP) as an oxidant [9,12]. The recognized effectiveness of molybdenum-based catalysts

for liquid phase epoxidation has led to the development of Mo catalysts with different architectures to meet superior performances in diverse reactions systems [13–15]. The ionic polymolybdates family of compounds has impressive structural diversity. They may be designed with different structural dimensionalities, types of anion and cations, etc. The primary units of the anions are $\{\text{MoO}_n\}$ coordination polyhedra (e.g., distorted $\{\text{MoO}_6\}$ octahedra or $\{\text{MoO}_4\}$ tetrahedra), which assemble in different fashions, leading to different nuclearities and types of metal and oxygen sites (e.g., internal or terminal sites, low high coordinate sites, different metal–oxygen distances and angles) [16]. On the other hand, the type of cations may influence the structural and chemical features such as interlayer distances and solubility properties of the ionic polymolybdates [17,18]. The different physicochemical properties of ionic polymolybdates may determine the catalytic performances [19,20].

Although there are relatively few literature studies on the topic, ionic polymolybdates with organic cations (IPOM) may be effective catalysts for upgrading FAMES [19,21–23], and they may be designed to meet superior catalytic performances. For example, a 2-D bis(anilinium) pentamolybdate, which possessed the simplest anilinium (Anil) cation, was a stable catalyst, although it possessed inferior activity to other 0-D and 1-D compounds, partly due to the presence of fewer accessible active sites in the 2-D structure [19]. Hence, the development of lower dimensionality Anil IPOM catalysts may lead to improved performances. On the other hand, IPOMs possessing the aliphatic counterpart of (aromatic) Anil, namely cyclohexylammonium (Cy6N), have not been reported to date, to the best of our knowledge. Cy6N may be less acidic than Anil [24] and influence the catalytic properties.

In this work, 0-D and 1-D IPOM compounds possessing the anions $[\text{Mo}_8\text{O}_{26}]^{4-}$ and $[\text{Mo}_3\text{O}_{10}]^{2-}$, and Cy6N or Anil as cations, were synthesized, characterised, and studied for liquid phase epoxidation systems, including FAMES conversion (Scheme 1). The IPOMs were cyclohexylammonium β -octamolybdate dihydrate (1), cyclohexylammonium trimolybdate hydrate (2), anilinium β -octamolybdate dihydrate (3), anilinium trimolybdate tetrahydrate (4) and anilinium trimolybdate dihydrate (5). The crystal structures of the new compounds 1, 2 and 5 were identified. The selected compounds possessed identical anions and different cations (e.g., 1/3, or 2/(4, 5)) or vice versa (1-2, or 3-6), and, on the other hand, include two pseudo-polymorphs (different hydrates) of anilinium trimolybdate (4, 5). The previously reported (stable) 2-D compound anilinium pentamolybdate (6) was included for comparative studies. The prepared compounds promoted olefin epoxidation with TBHP. To the best of our knowledge, 1 and 2 are the first molybdenum compounds with a cyclohexylamine-type organic component reported for catalytic epoxidation. The reaction scope of applications of the IPOM catalysts included cyclooctane oxidation.



Scheme 1. Olefin epoxidation reaction systems studied for the IPOM catalysts 1–6, using TBHP as oxidant, at 70 °C, and the respective kinetic constants (k_i) per step.

2. Results and Discussion

2.1. Structures of the IPOM Catalysts

Table 1 summarises the structural dimensionality and chemical formulae of the IPOM compounds 1–5, and, for comparison, 6. The most important crystallographic data for the new compounds 1, 2 and 5, based on single crystal methods, are indicated in Table 2, and further details are given in Tables S1–S3.

Table 1. Structural dimensionality and chemical formulae of compounds 1–6.

	Chemical Name	Chemical Formula	Structural Features	Dim ^a	Dx/DC ^b	n(oxo)/Mo ^c
1	Cyclohexylammonium β -octamolybdate dihydrate	(C ₆ H ₁₄ N) ₄ [Mo ₈ O ₂₆]·2H ₂ O	isolated clusters	0-D	2.264/ 4	1.75
2	Cyclohexylammonium trimolybdate hydrate	(C ₆ H ₁₄ N) ₂ [Mo ₃ O ₁₀]·H ₂ O	polymeric	1-D	2.056/ 3	2
3	Anilinium β -octamolybdate dihydrate	(C ₆ H ₈ N) ₄ [Mo ₈ O ₂₆]·2H ₂ O	isolated clusters	0-D	2.520/ 4	1.75
4	Anilinium trimolybdate tetrahydrate	(C ₆ H ₈ N) ₂ [Mo ₃ O ₁₀]·4H ₂ O	polymeric	1-D	2.180/ 3	2
5	Anilinium trimolybdate dihydrate	(C ₆ H ₈ N) ₂ [Mo ₃ O ₁₀]·2H ₂ O	polymeric	1-D	2.399/ 3	2
6	Anilinium pentamolybdate	(C ₆ H ₈ N) ₂ [Mo ₅ O ₁₆]	layered	2-D	2.850/ 5	0.8

^a Dim. = structural dimensionality. ^b Dx = calculated density (by X-ray diffraction technique) and DC = degree of condensation, which, for isopolymolybdates, equals (number of Mo atoms)/(0.5 × (cluster charge)); DC represents the number of Mo atoms in the polymolybdate formula written in the form M(I)₂O_x.xMoO₃, where M(I) represents a monovalent metal cation. ^c Number (n(oxo)) of oxo groups (terminal oxygen atoms) per Mo atoms of the anion.

A search into the crystallographic database for 1 indicated that it is a new polymorphic modification of cyclohexylamine β -octamolybdate. In comparison to a previously reported monoclinic C-centred structure [25], a much smaller triclinic structure was obtained for 1 (i.e., it is not a simple subgroup of the previously reported monoclinic compound, as may be confirmed by the Checkcif reports). An essential building unit (with labelling scheme) and packing of the molecules are presented in Figure 1a and b, respectively, and a simplified representation of how the structure is built is presented in Figure 1c. The β -octamolybdate anion can be summarized as a polyoxometalate ion (IPOM) formed by 8 Mo atoms and 26 O atoms, among which there exist 14 terminal O atoms (Mo=O with \sim 1.707(8) Å length), 6 O atoms of μ_2 type, 4 O atoms of μ_3 type and 2 O atoms of μ_5 type.

Table 2. Summary of crystal data of the new compounds 1, 2 and 5.

Compound (XRD Technique)	1 (Single Crystals)	2 (Powder Data)	5 (Powder Data)
Chemical formula	C ₂₄ H ₆₀ Mo ₈ N ₄ O ₂₈	C ₁₂ H ₃₀ Mo ₃ N ₂ O ₁₁	C ₁₂ H ₂₀ Mo ₃ N ₂ O ₁₂
MW (g/mol)	1620.27	666.20	672.12
T(K)	100	293(2)	293(2)
Wavelength, [Å]	MoK α : 0.71073	CuK α : 1.54187	CuK α : 1.54187
Crystal system, space group	triclinic, P-1	Orthorhombic, P nma	Monoclinic, P 2 ₁ /c
Cell parameters			
a [Å]	8.7255(2)	8.763(3)	14.711
b [Å]	10.5278(2)	7.645(3)	7.578
c [Å]	14.4778(4)	32.114(4)	17.852
α [°]	75.019(2)	90	90
β [°]	76.273(2)	90	110.81
γ [°]	69.550(2)	90	90
V (Å ³)	1187.79(5)	2151.4(4)	1860.31
Z, calculated density (g/cm ³)	1, 2.264	4, 2.056	4, 2.399
Absorption coefficient (mm ⁻¹)	12.775	14.627	16.959 na
F(000)	792	1200	996
2Theta range	5.04–31.9363.86	3.5–80	3.5–70
Limiting indices	-12 ≤ h ≤ 12; -15 ≤ k ≤ 15; -20 ≤ l ≤ 21	7; 6; 26	10; 5; 13
Reflections collected	7841	524	526

Table 2. Cont.

Compound (XRD Technique)	1 (Single Crystals)	2 (Powder Data)	5 (Powder Data)
Completeness to theta(max)	95.5%	100% (xrpd)	100% (xrpd)
Absorption correction	Multi-scan	const. (Bragg-Brentano geom.)	const. (Bragg-Brentano geom.)
Maximum and minimum transmission	n.a. (powder sample)		
Refinement method	wR2	Rietveld	Rietveld
Data/restraints/parameters	7841/0/321	3824/36/25	3325/30/20
Goodness of fit on F2	1.23	8	11
Final R indices			
wR2 ($I > 2\sigma$) or R_p/R_{wp}	8.70	22.8/26.0	15.1/20.9
R_f (all data)	3.15	14.29	19.11
Largest difference peak and hole ($e\text{\AA}^{-3}$)	1.612/−1.447	PD	PD
CCDC	2,320,511	PD−1	PD−1

^{PD} Usually not reported in XRPD studies. ^{PD−1} Submitted to ICDD to supplement deposited data.

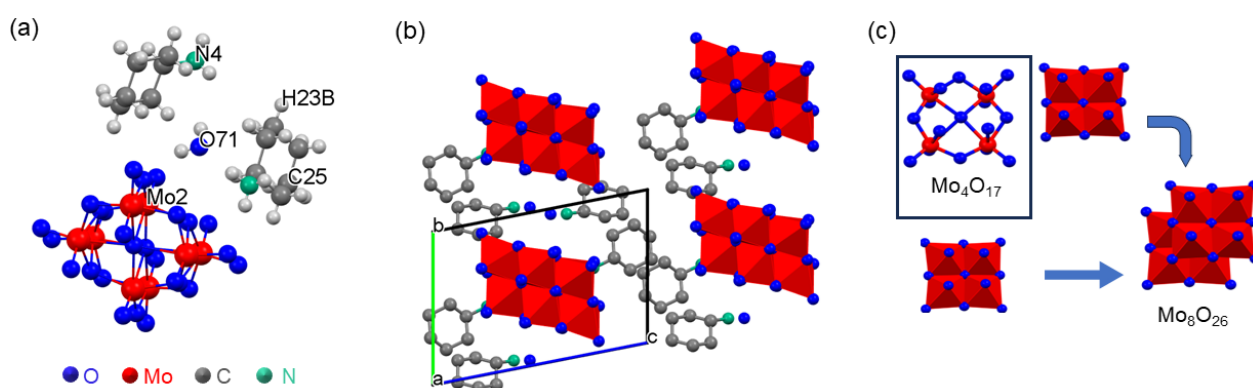


Figure 1. (a) Essential building unit (with labelling scheme), (b) packing of the molecules and (c) simplified representation how the structure is built for 1.

Compound 2 is a new trimolybdate of cyclohexylammonium, which is crystallized (fibrillar crystals) in an orthorhombic system. Polymeric anionic chains of Mo_3O_{10} stoichiometry (monomers) are built of distorted $\{\text{MoO}_6\}$ octahedra, linked together by edges and vertices. By sharing one edge, the two octahedra form Mo_2O_{10} groups, and by sharing the vertices, these groups form infinite double chains of Mo_2O_8 units. This ribbon is joined by alternate MoO_6 octahedra (on both sides of it). The resultant composition is Mo_3O_{10} , and the length of the identity period along the polymer axis is equal to two heights of the MoO_6 octahedron ($2 \times 3.8 = 7.6 \text{ \AA}$). In each octahedron, there exist two terminal O atoms, and four O of μ_3 type. Between chains running along the $[010]$ direction, there exist molecules of protonated amines, and water. The essential building unit (with labelling scheme) and packing of the molecules for 2 are presented in Figures 2a and 2b, respectively, and a simplified representation of how the structure is built is presented in Figure 2c.

For the new 1-D compound 5, a similar arrangement of inorganic polymeric chains to that of compound 2 was obtained; the molecular packing is given in Figure 3. However, the monoclinic structure of 5 was slightly denser than the orthorhombic structures of 2 and 4 (Table 1). The calculated density (D_x) equals 2.399 for 5 versus 2.180 and 2.056 for 4 and 2, respectively (Table 1). Based on a comparison for all IPOM compounds, the D_x was highest for the 2-D 6, which is a layered material with infinite anionic layers $[(\text{Mo}_5\text{O}_{16})^{2-}]_n$ formed by distorted MoO_6 octahedra [26].

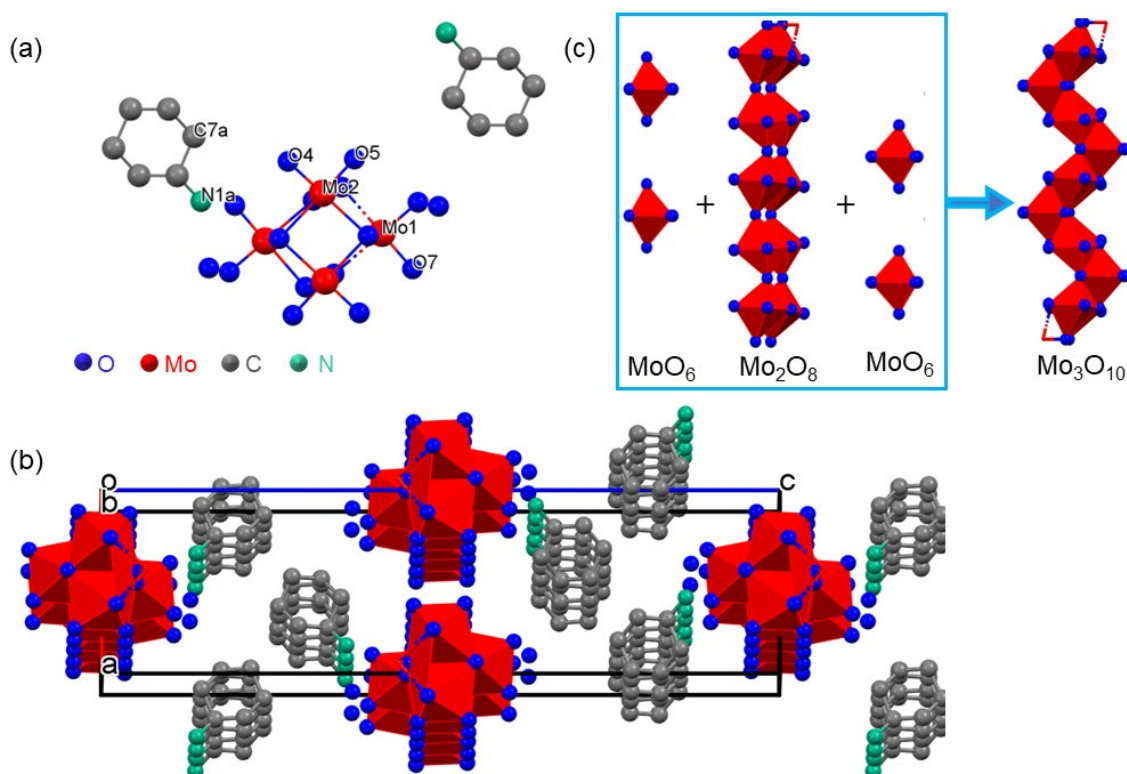


Figure 2. (a) Essential building unit (with labelling scheme), (b) packing of the molecules and (c) simplified representation how the structure is built for 2.

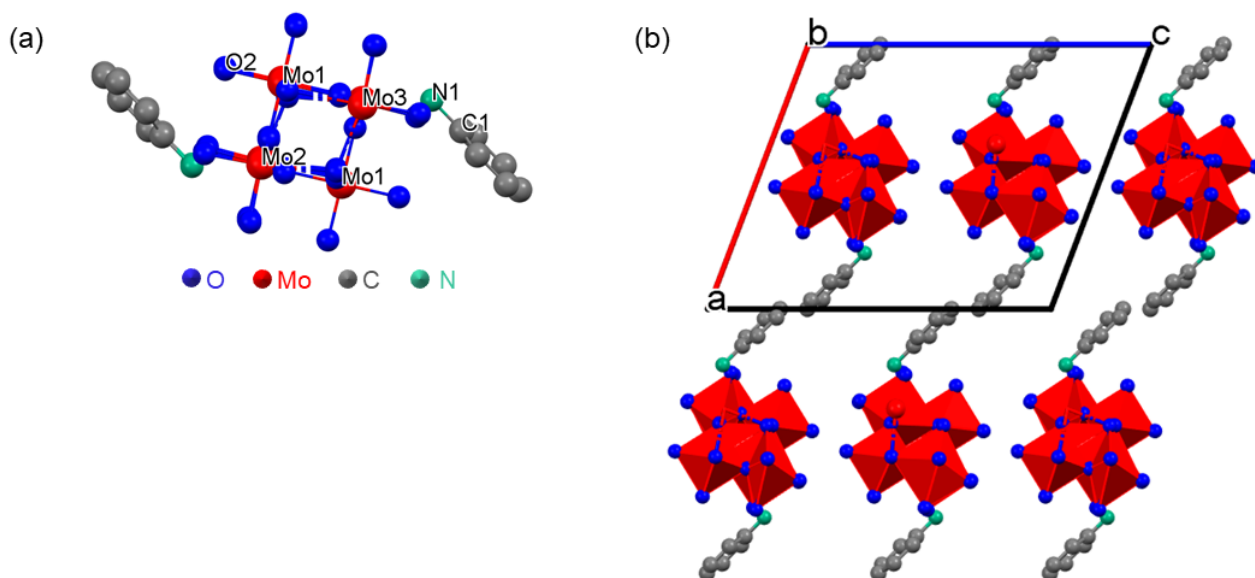


Figure 3. (a) Essential building unit (with labelling scheme), and (b) packing of the molecules for 5.

The variable temperature X-ray powder diffraction (XRPD/temp) and thermal analyses (TG/DSC) results for 1, 2 and 5 are given in the Supporting information (Figures S1–S3 and S4–S6). The corresponding data for the remaining compounds was previously reported by some of us [26]. In general, octamolybdates (0-D) seem slightly more thermally stable than the trimolybdates (1-D), and layered (2-D) pentamolybdates appeared to be the most stable. Through prolonged heating, the anilinium trimolybdate tetrahydrate 4 (which was synthesized in aqueous conditions) converted completely to a solid with same crystal structure as that of 5. Importantly, compounds

1–6 are thermally stable in the temperature range of the catalytic studies reported in this work (up to 120 °C).

The structural dimensionality seems to be essentially related to the type of anion: 0-D for $[\text{Mo}_8\text{O}_{26}]^{4-}$, 1-D for $[\text{Mo}_3\text{O}_{10}]^{2-}$ and 2-D for $[\text{Mo}_5\text{O}_{16}]^{2-}$. On the other hand, depending on the type of anion, the IPOMs possess different amounts of terminal oxygen atoms ($\text{Mo}=\text{O}$) per total amount of molybdenum atoms ($n(\text{oxo})/\text{Mo}$), which equals 2 for trimolybdates (1-D), 1.75 for octamolybdates (0-D) and 0.8 for pentamolybdates (2-D) (Table 1). For each family of IPOMs, the $n(\text{oxo})/\text{Mo}$ ratio increased with decreasing density Dx (Figure 4).

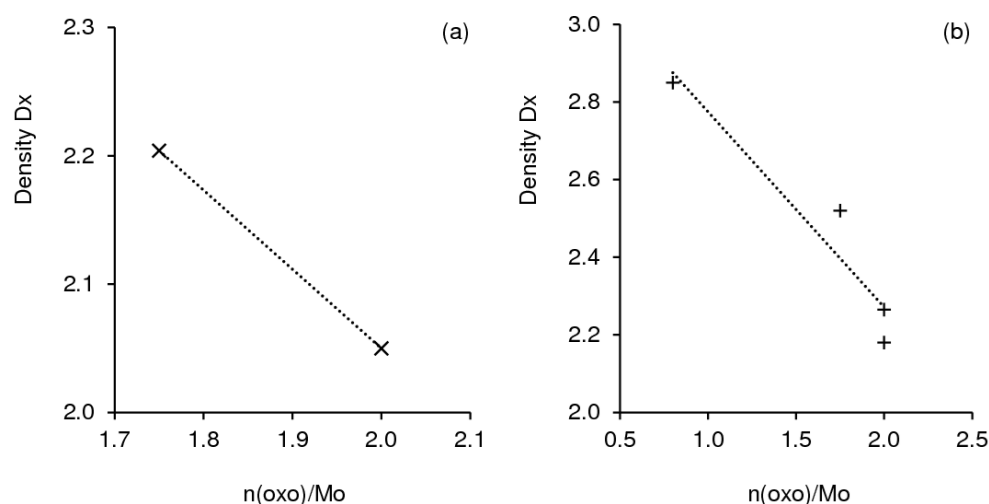


Figure 4. Relationship between Dx and the ratio $n(\text{oxo})/\text{Mo}$ for the Cy6N (a) and Anil (b) families of IPOM compounds.

2.2. Catalytic Studies

2.2.1. Olefin Epoxidation

Impact of IPOM Features

The IPOM catalysts were firstly compared based on the model reaction of *cis*-cyclooctene (Cy) with *tert*-butyl hydroperoxide (TBHP) at 70 °C. The initial molar ratios of Mo:olefin and Mo:TBHP were kept constant in all catalytic tests, i.e., the catalytic performances were compared on the basis of the same amount of molybdenum in the reactors. Cyclooctene oxide (CyO) was the only product formed for all catalytic tests (Scheme 1). Blank reactions without catalyst and/or without TBHP led to negligible Cy conversion at 24 h, indicating the need for both a molybdenum catalyst and TBHP for the epoxidation reaction to occur. It is consensual from the literature that molybdenum-catalysed epoxidation of olefins occurs via a heterolytic mechanism which may be initialised via the coordination of the hydroperoxide oxidant (TBHP) to the Lewis acid metal centre, leading to active oxidising species. The latter species are responsible for the oxygen atom transfer to the olefin, giving the corresponding epoxide product plus *tert*-butanol, which is the coproduct of TBHP [27–30]. The types of active oxidising species may possess a $\{\text{Mo}(\text{OH})(\text{OO}t\text{Bu})\}$ (*t*Bu = *tert*-butyl) moiety, and its formation involves a oxomolybdenum ($\text{Mo}=\text{O}$) group [27–30].

Figure 5 compares the catalytic results for the IPOM compounds based on Cy conversions at different reaction times. The catalytic results were similar for the pseudo-polymorphs (different hydrates) of anilinium trimolybdate (4 and 5); 100% Cy conversion at 1 h. These results were correlated with the identical anions and cations (independently of the extent of hydration) of 4 and 5. On the other hand, a comparative study of the IPOMs with the same type of anion (and structural dimensionality) but different cations suggested that the anilinium (Anil) family (3, 4, 5) was more active than the cyclohexylamine (Cy6N) one (1, 2). Specifically, the Anil IPOMs led to 100% Cy conversion within 1 h, whereas for the Cy6N ones (1, 2), the reaction was complete only after 4 h (1 vs. 3, and 2 vs. 4 and 5).

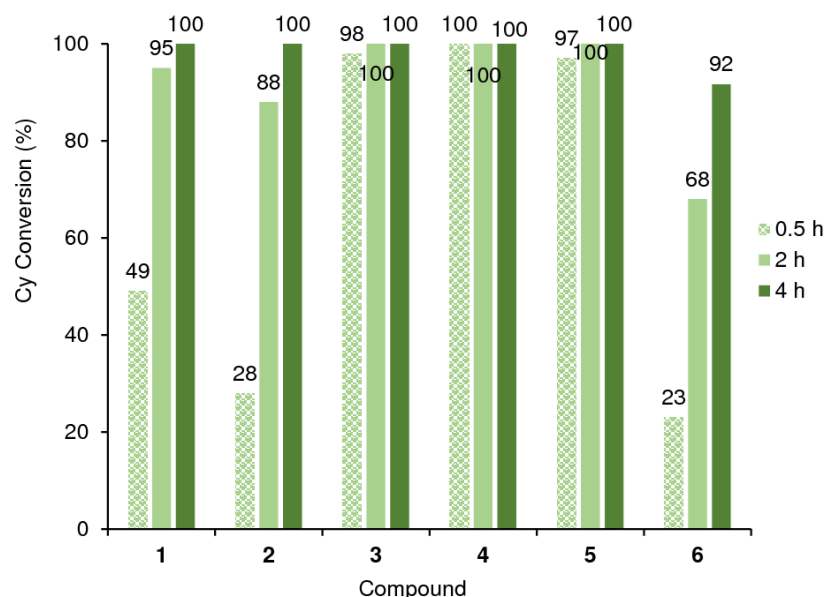


Figure 5. *cis*-Cyclooctene (Cy) epoxidation with TBHP, in the presence of 1–6, at 70 °C. Epoxide selectivity was always 100%.

Catalysts **3**, **4** and **5** remained very active at the lower reaction temperature of 55 °C; 63, 87 and 100% Cy conversion was achieved, respectively, at 1 h (Figure S14). Catalyst **5** led to superior results (based on Cy conversion at 1 h, 55 °C) to literature data for IPOMs possessing different anilinium type cations, namely 1-D ($C_8H_{12}N$)₂[Mo₃O₁₀] (91%) and 1-D ($C_7H_{10}N$)₂[Mo₃O₁₀] (71%) (Table S6) [19].

The reaction mixtures were biphasic solid–liquid. High Cy conversions were reached in the initial stages (38–100% within 30 min reaction, in the presence of 1–5). The recovered solids 1–5 were reused and led to roughly comparable catalytic results to the respective original catalysts (Figure 6). The characterisation studies of the used catalysts suggested that the chemistry (ATR FT-IR spectroscopy) and crystalline structures (XRPD) seemed to be preserved (similar characterisation results were obtained for the fresh and used catalysts, Figure S16). This parallels that reported for compound **6** [19]. Hence, the constituent ions seem to withstand the catalytic reaction conditions. Nevertheless, one cannot exclude contributions of dissolved metal species. Contact tests were carried out for 1–6, which suggested that the catalytic reactions were essentially homogeneous (details in experimental section; Figure S15). Attempts to precipitate dissolved species (please see details in the experimental section, for 1–5) did not lead to measurable (or visible) amounts, suggesting that the dissolved fractions were very soluble.

The catalytic performances may depend on the interplay of several factors, such as the type of organic cation, ratio ($n(\text{oxo})/\text{Mo}$), and/or catalyst solubility. Based on the above mechanistic considerations, more available Mo=O groups may favour the epoxidation reaction kinetics, since the reaction begins with the coordination of the oxidant to a metal centre (of the anion) with the concomitant protonation of an oxomolybdenum group (Mo=O) [27–30]. On the other hand, one cannot exclude the possibility of the structural properties of the IPOMs (e.g., Dx) influencing the kinetics of dissolution of metal species, and consequently the overall epoxidation reaction kinetics (which is essentially homogeneous). In this sense, Figure S17 shows the kinetic constants (Table 3; Supplementary Materials for kinetic modelling details) as a function of Dx or $n(\text{oxo})/\text{Mo}$ ratio. For the Anil family, **4** and **5**, which possessed lower Dx (and higher $n(\text{oxo})/\text{Mo}$, Table 1) than **3**, led to faster reaction kinetics ($k_{\text{Cy}} = 11.5946$ and 10.9802 h^{-1} for **4** and **5**, respectively, and $k_{\text{Cy}} = 6.3279$ for **3**, Table 3). Compound **6**, with the highest Dx (and lowest $n(\text{oxo})/\text{Mo}$, Table 1), led to the slowest reaction kinetics ($k_{\text{Cy}} = 0.5565 \text{ h}^{-1}$ for **6** versus 1.0774 – 11.5946 h^{-1} for the remaining catalysts). However, the opposite was verified for the Cy6N family.

Specifically, **1**, with higher D_x (and lower $n(\text{oxo})/\text{Mo}$), led to faster reaction kinetics than **2** ($k_{\text{Cy}} = 1.3989$ and 1.0774 h^{-1} , respectively). Hence, D_x does not solely explain the observed differences of reaction kinetics. Another possible factor is the different structural dimensionalities of the IPOMs, since a lower structural dimensionality may facilitate dissolution of metal species, and consequently the overall reaction. This could partly explain the catalytic differences between **1** (0-D) and **2** (1-D) but does not explain the differences observed for all compounds. The above results suggest that the (yet unknown) soluble active metal species may be structurally different for the different IPOMs, contributing with different intrinsic activities to the overall reaction.

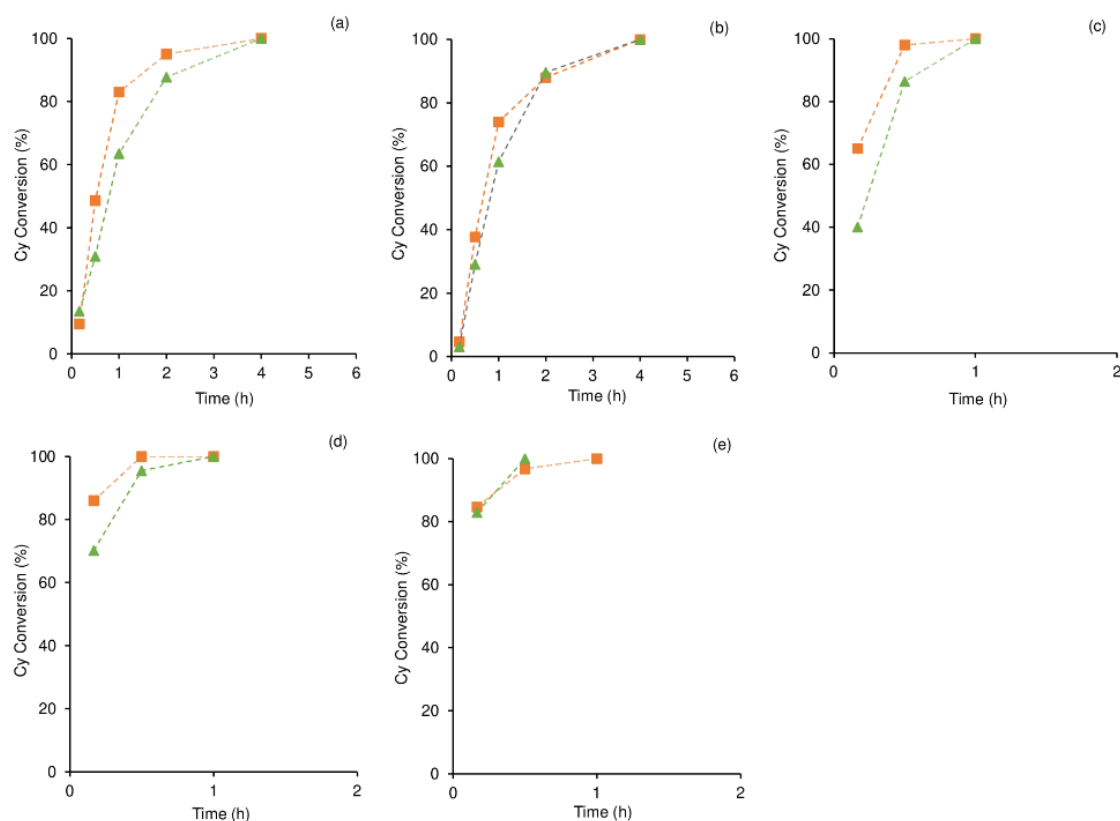


Figure 6. First (■) and second (▲) catalytic runs of *cis*-cyclooctene (Cy) epoxidation with TBHP, in the presence of **1** (a), **2** (b), **3** (c), **4** (d) and **5** (e), at 70 °C. Epoxide selectivity was always 100%.

Table 3. Kinetic constants (k_i) and objective function (F_{obj}) obtained from the kinetic models for Cy, Ole and Lin reactions, in the presence of the IPOM catalysts, at 70 °C.

k_i (h^{-1})	Reaction	1	2	3	4	5	6
k_{Cy}	Cy-CyO	1.3989	1.0774	6.3279	11.5946	10.9802	0.5565
F_{obj}		4.05×10^{-2}	4.70×10^{-2}	1.20×10^{-3}	2.00×10^{-5}	1.60×10^{-3}	1.88×10^{-2}
k_{Ole}	Ole-OleOx	0.5356	0.3002	2.4035	3.1423	2.4031	0.3149
F_{obj}		5.61×10^{-2}	2.27×10^{-2}	4.26×10^{-4}	3.33×10^{-6}	6.24×10^{-4}	2.76×10^{-2}
$k_{\text{Lin},1}$	Lin-LinOx	0.5827	0.4767	0.6392	0.7294	0.7607	0.3957
$k_{\text{Lin},2}$	LinOx-LinDiOx	0.1262	0.1087	0.1888	0.2248	0.2191	0.0893
$k_{\text{Lin},3}$	LinDiOx-LinFur	0.0594	0.0013	0.2527	0.2811	0.2594	0.0647
F_{obj}		5.20×10^{-2}	7.20×10^{-2}	1.36×10^{-2}	7.48×10^{-2}	6.70×10^{-2}	7.00×10^{-2}

Table 4 compares the catalytic results for **1–6** to literature data for different IPOMs possessing anilinium derivatives as organic components. To the best of our knowledge, there are no literature studies on IPOM epoxidation catalysts possessing cyclohexylammonium derivatives as organic components. A comparative study for the anilinium family (entries

4, 5, 7 and 8), suggested that the 1-D catalysts are highly active, and, on the other hand, the 2-D catalysts (entries 6 and 9–11) seemed generally less active than the 1-D ones.

Table 4. Comparison of the catalytic results for 1–6 to literature data for IPOM compounds possessing anilinium derivatives as organic components, tested for the Cy/TBHP reaction at 70 °C ^a.

#	Catalyst	Dim. ^b	t (h) ^c	Conv., CyO yield (%) ^d	Ref.
1	1	0-D	1/2/4	83/95/100	-
2	2	1-D	1/2/4	74/88/100	-
3	3	0-D	0.5/1	98/100	-
4	4	1-D	0.5	100	-
5	5	1-D	0.5/1	97/100	-
6	6	2-D	1/4	48/86	[19]
7	(C ₈ H ₁₂ N) ₂ [Mo ₃ O ₁₀]	1-D	1/6	97/100	[19]
8	(C ₇ H ₁₀ N) ₂ [Mo ₃ O ₁₀]	1-D	1	100	[19]
9	(C ₈ H ₁₂ N) ₂ [Mo ₅ O ₁₆]	2-D	1/6	54/98	[19]
10	(C ₇ H ₁₀ N) ₂ [Mo ₅ O ₁₆]	2-D	1/6	40/94	[19]
11	(C ₈ H ₁₂ N) ₂ [Mo ₅ O ₁₆]	2-D	1/6	44/92	[19]

^a Initial molar ratio Mo:olefin:oxidante = 1:100:153. ^b Dim. = Structural dimensionality. ^c t = Reaction time.

^d Conv. = Cy conversion, CyO yield = cyclooctene oxide yield (epoxide selectivity was 100%).

Biobased Olefin Epoxidation

The synthesized IPOMs were further explored for the epoxidation of FAMES, namely monounsaturated methyl oleate (Ole) and double unsaturated methyl linoleate (Lin), with TBHP, at 70 °C. All catalysts led to 100% Ole conversion within 24 h, and the epoxide 9,10-epoxyoctadecanoate (OleOx) was formed with 100% selectivity. Without catalyst, the reaction was sluggish (12% Ole conversion at 24 h).

The reaction kinetics depended on the type of IPOM catalysts. The Anil family of compounds 3–5 was more active than the Cy6N one (Figure 7), in parallel to the results verified with Cy as the substrate (Figures 5 and S17). For the Cy6N family, 1 led to a faster reaction than 2 ($k_{\text{Ole}} = 0.5356$ and 0.3002 h^{-1} , respectively, Table 3; kinetic curves in Figure S12). On the other hand, for the Anil family, the reaction kinetics was faster for 3–5 ($k_{\text{Ole}} = 2.4031$ – 3.1423 h^{-1}) than 6 ($k_{\text{Ole}} = 0.3149 \text{ h}^{-1}$). Ole conversion at 2 h was 95–100% for 3–5 and only 43% for 6. After 2 h reaction, the differences in kinetic profiles were less pronounced (Figure S12), e.g., at 4 h and 24 h, 1–5 led to 81–84% and 96–100% Ole conversion, respectively.

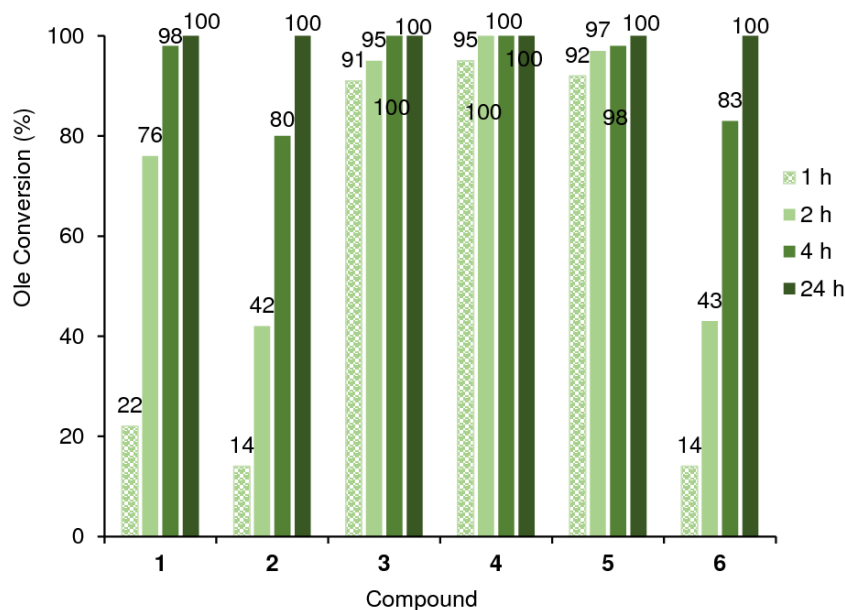


Figure 7. Methyl oleate (Ole) epoxidation with TBHP, in the presence of 1–6, at 70 °C. Epoxide selectivity was always 100%.

Based on a literature survey for IPOM catalysts tested for the target reaction (Ole/TBHP), it seems that, in general, 3–5 performed superiorly to other catalysts (Table 5). The 1-D compound bis(3,5-dimethylanilinium) trimolybdate ((C₈H₁₂N)₂[Mo₃O₁₀]) led to 84% OleOx yield at 89% Ole conversion at 6 h (70 °C), which is inferior to the 1-D 3–5 IPOMs (91–95% Ole conversion at 1 h; entry 7 vs. entries 3–5, Table 5) [19]. The introduction of alkyl substituent groups in the anilinium cation did not seem to improve the catalytic performance, which may be partly due to differences in catalyst solubility and/or acid–base properties of the anilinium derivatives [31]. The 0-D pyridinium-tetrazole-based polyoxometallates (Hptz)₄[SiMo₁₂O₄₀]·nH₂O and (tBu-ptz)₂[Mo₆O₁₉] performed differently under somewhat comparable reaction conditions, with the latter being less active (88% Ole conversion at 6 h) than the former (97% Ole conversion at 3 h) (entries 8 and 9) [32,33]. Both compounds were less active than 3–5. At a higher temperature (75 °C), the clusters (py)₄[Mo₈O₂₆] and (tBu-py)₄[Mo₈O₂₆] (py = pyridine, tBu-py = 4-*tert*-butylpyridine) led to ca. 97%/99% OleOx yield after 2 h/6 h reaction (entries 10 and 11) [23].

Table 5. Comparison of the catalytic results for 1–6 to literature data for IPOM compounds tested for the Ole/TBHP reaction.

#	Catalyst ^a	Dim. ^b	Reaction Conditions ^c				Conv. ^d (%)	OleOx Yield (%)	Ref
			Solv.	T (°C)	Mo:S:ox	t (h)			
1	1	0-D	TFT	70	1:100:300	½/4	22/76/98	22/74/96	-
2	2	1-D	TFT	70	1:100:300	½/4	14/42/80	14/42/80	-
3	3	0-D	TFT	70	1:100:300	½/4	91/97/100	91/97/100	-
4	4	1-D	TFT	70	1:100:300	½	95/100	95/100	-
5	5	1-D	TFT	70	1:100:300	½/4	92/97/98	92/97/98	-
6	6	2-D	TFT	70	1:100:300	½/4/24	14/43/83/100	14/43/83/96	-
7	(C ₈ H ₁₂ N) ₂ [Mo ₃ O ₁₀]	1-D	TFT	70	1:100:153	1/6/24	70/89/99	66/84/92	[19]
8	(Hptz) ₄ [SiMo ₁₂ O ₄₀]·nH ₂ O	0-D	TFT	70	1:100:250	1/6/24	56/88/100	56/88/100	[32]
9	(tBu-ptz) ₂ [Mo ₆ O ₁₉]	0-D	TFT	70	1:100:210	0.5/3	73/97	73/97	[33]
10	(py) ₄ [Mo ₈ O ₂₆]	0-D	DCE	75	1:100:152	2/6	~97/100	~97/99	[23]
11	(tBu-py) ₄ [Mo ₈ O ₂₆]	0-D	DCE	75	1:100:152	2/6	~97/100	~97/99	[23]

^a ptz = 5-(2-pyridyl)tetrazole; tBu-ptz = 2-*tert*-butyl-5-(2-pyridyl)-2H-tetrazole; py = pyridine; tBu-py = 4-*tert*-butylpyridine. ^b Dim. = structural dimensionality. ^c Solv. = solvent; TFT = α,α,α-trifluorotoluene, DCE = 1,2-dichloroethane; Mo:S:ox = initial molar ratio of molybdenum:substrate:oxidant; T = reaction temperature; t = time. ^d Conv. = Ole conversion.

IPOMs 1–6 promoted the epoxidation of methyl linoleate (Lin) with TBHP, leading to 98–100% Lin conversion within 24 h (Figure 8); the kinetic constants were greater for 3–5 than 1–2 (Table 3; calculated kinetic curves in Figure S13). The products were monoepoxides, diepoxides and furan-type compounds (Scheme 1, Figure 9). The monoepoxides methyl-9,10-epoxy-12-octadecenoate and 12,13-epoxy-9-octadecenoate (LinOx) were formed initially. LinOx selectivity decreased with increasing Lin conversion, which was accompanied by the formation of the diepoxides methyl 9,10-12,13-diepoxyoctadecanoate (LinDiOx) and the furanic products methyl 10,13-epoxy-9,12-dihydroxyoctadecanoate and methyl 9,12-epoxy-10,13-dihydroxyoctadecanoate (LinFur) (Figure 9). The LinFur products may be formed via epoxide ring opening of LinDiOx and intramolecular cyclization [34–37]. According to the literature, due to the proximity of the two epoxide groups (separated by a -CH₂ group), the ring opening of one of these groups may give unstable intermediates which rapidly undergo cyclization to LinFur [34–37].

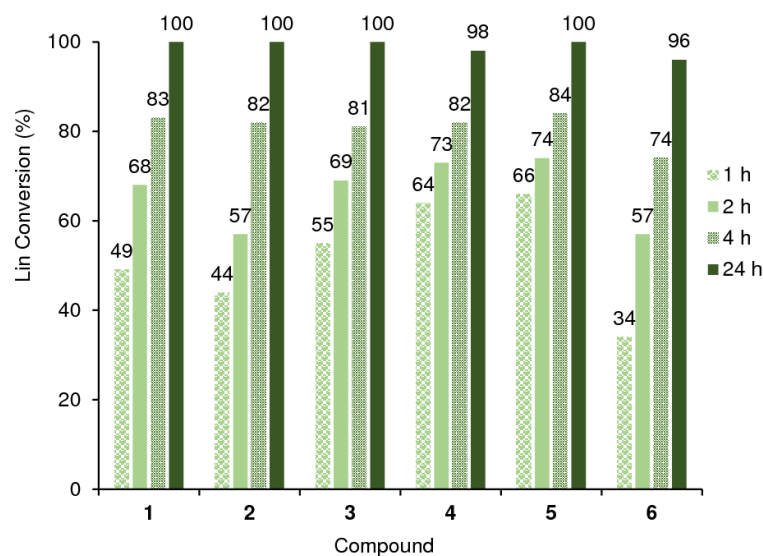


Figure 8. Methyl linoleate (Lin) epoxidation with TBHP, in the presence of 1–6, at 70 °C.

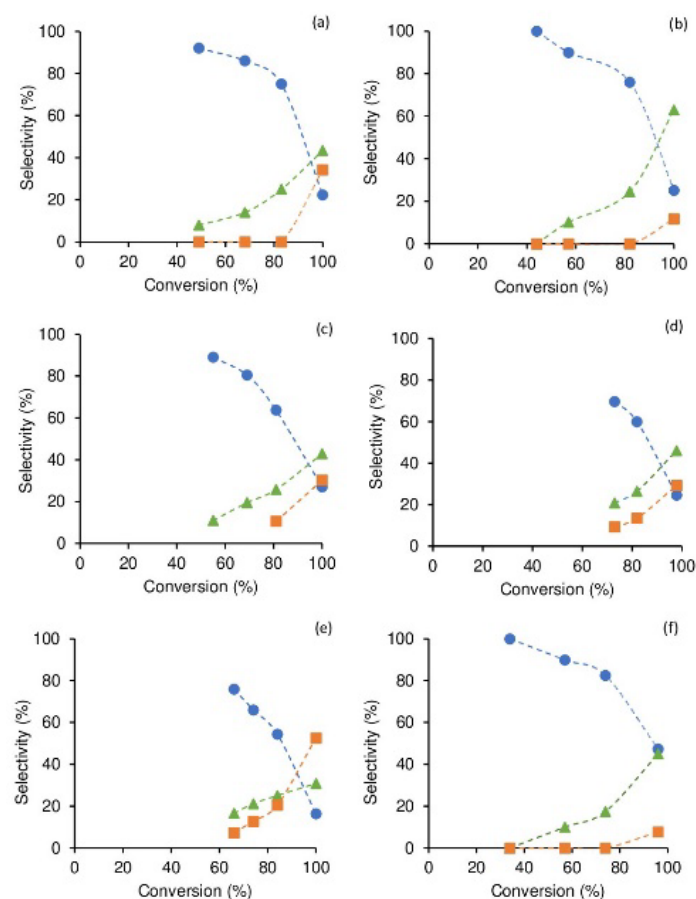


Figure 9. Dependency of products selectivity on methyl linoleate (Lin) conversion (LinOx (●), LinDiOx (▲) and LinFur (■)), in the presence of 1 (a), 2 (b), 3 (c), 4 (d), 5 (e) and 6 (f), at 70 °C.

Table 6 compares the catalytic results for 1–6 to literature data for IPOM type catalysts tested for the Lin reaction. The 1-D bis(3,5-dimethylanilinium) trimolybdate ($C_8H_{12}N)_2[Mo_3O_{10}]$ led to 39% LinOx yield, 39% LinDiOx yield and 16% yield LinFur at 95% Lin conversion (70 °C, 24 h, molar ratio Mo:LinOle:TBHP = 1:100:250) [19]. Under somewhat similar reaction conditions to those used for 1–6, the catalyst $(Hptz)_4[SiMo_{12}O_{40}] \cdot nH_2O$ (ptz = 5-(2-pyridyl)tetrazole) led to 60%/28% LinOx selectivity, 31%/33% LinDiOx selectivity and 9%/40% LinFur selectivity at

87%/100% Lin conversion (6 h/24 h) [32]. On the other hand, only epoxides were formed for a related ionic compound with a substituted ptz organic fragment (*t*Bu-Hptz)₂[Mo₆O₁₉], which led to 83% LinOx and 17% LinDiOx selectivity at 85% Lin conversion, 24 h/70 °C [33]. For this catalyst, the selectivity towards epoxides remained high at 90 °C (63% and 37% of LinOx and LinDiOx selectivity, respectively, at 100% Lin conversion, 2 h), and no LinFur products were formed [33].

Table 6. Comparison of the catalytic results for 1–6 to literature data for IPOM compounds tested for the Lin/TBHP reaction.

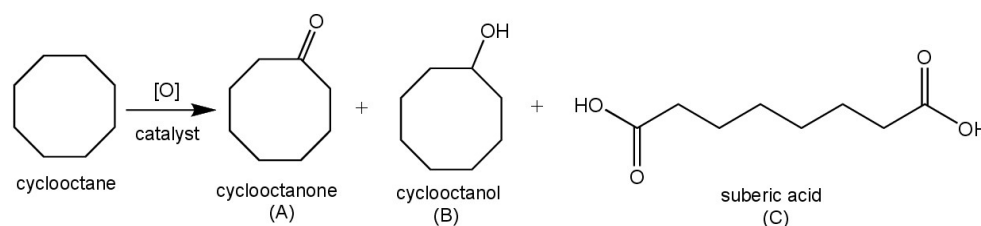
Catalyst ^a	Reaction Conditions ^b			Conv. (%) ^c	Selectivity (%)			Ref.
	Solv.; T (°C)	Mo:S:ox	t (h)		LinOx	LinDiOx	LinFur	
1	TFT; 70	1:100:300	1/4/24	49/83/100	92/75/23	8/25/43	0/0/34	-
2	TFT; 70	1:100:300	1/4/24	44/82/100	100/76/25	0/24/63	0/0/12	-
3	TFT; 70	1:100:300	1/4/24	55/81/100	89/64/27	11/25/43	0/11/30	-
4	TFT; 70	1:100:300	1/4/24	64/82/98	77/60/25	18/27/46	5/13/29	-
5	TFT; 70	1:100:300	1/4/24	66/84/100	76/54/16	17/25/31	7/21/53	-
6	TFT; 70	1:100:300	1/4/24	34/74/96	100/82/47	0/18/45	0/0/8	-
(C ₈ H ₁₂ N) ₂ [Mo ₃ O ₁₀]	TFT; 70	1:100:250	24	95	41	41	17	[19]
[<i>t</i> Bu-Hptz] ₂ [Mo ₆ O ₁₉]	TFT; 70	1:100:210	0.5/24	36/85	100/83	0/17	0	[33]
[<i>t</i> Bu-Hptz] ₂ [Mo ₆ O ₁₉]	TFT; 90	1:100:210	0.5/2	80/100	81/63	19/37	0	[33]
(Hptz) ₄ [SiMo ₁₂ O ₄₀]. <i>n</i> H ₂ O	TFT; 70	1:100:250	1/6/24	45/87/100	100/60/28	0/31/33	0/9/40	[32]

^a *t*Bu-ptz = 2-*tert*-butyl-5-(2-pyridyl)-2H-tetrazole; ptz = 5-(2-pyridyl)tetrazole. ^b Solv. = solvent; TFT = α,α,α -trifluorotoluene, Mo:S:ox = initial molar ratio of molybdenum:substrate:oxidant, T = reaction temperature, t = time. ^c Conv. = Lin conversion.

In summary, there have been few ionic molybdenum compounds tested for Lin reaction, and the results for 3–5 seem promising. Outstandingly, 5 led to the highest LinFur yield (Table 6). The conversion of FAMES to higher polarity products such as LinFur may further broaden the applications profile of FAMES [34], e.g., there is an increasing interest in substituted tetrahydrofurans as potential plasticizers, antibiotics and antitumour, pesticidal, antiprotozoal and antimicrobial agents [38–41].

2.2.2. Cyclooctane Oxidation

The prepared IPOMs were further explored for the oxidation of cyclooctane in air at 10 atm and 120 °C (Table 7, Scheme 2). The main products were cyclooctanone (A) and cyclooctanol (B), and to a lower extent, suberic acid (C), which were formed in a similar molar ratio (A + B)/(A + B + C) of 0.80–0.86, at 6 h. According to the literature, cyclooctane oxidation in the presence of IPOMs may occur via homolytic mechanism [26].



Scheme 2. Cyclooctane oxidation, in the presence of the IPOMs 1–6, at 120 °C.

Table 7. Comparison of the catalytic results for 1–6 to literature data for IPOMs possessing anilinium derivatives as organic components, tested for the cyclooctane/O₂ reaction at 120 °C ^a.

Catalyst	Dim	Ketone Yield (A) (%)	Alcohol Yield (B) (%)	Suberic Acid Yield (C) (%)	Conv. ^b (%)	A/B	(A + B)/(A + B + C)	Ref.
1	0-D	35	13	8	56	2.29	0.86	-
2	1-D	41	13	12	66	3.15	0.82	-
3	0-D	37	14	13	64	2.64	0.80	-
4	1-D	41	15	11	67	2.73	0.83	-
5	1-D	39	14	11	64	2.79	0.83	-
6	2-D	27	11	8	46	2.45	0.83	-
(C ₇ H ₁₀ N) ₄ [Mo ₈ O ₂₆]·2H ₂ O	0-D	11	9	0	20	1.14	1.00	[26]
(C ₈ H ₁₂ N) ₂ [Mo ₃ O ₁₀]	1-D	30	16	0	46	1.91	1.00	[26]
(C ₇ H ₁₀ N) ₂ [Mo ₃ O ₁₀]	1-D	26	16	0	42	1.61	1.00	[26]
(C ₇ H ₁₀ N) ₂ [Mo ₅ O ₁₆]	2-D	34	11	~5	~50	3.16	~0.90	[26]
(C ₆ H ₇ NBr) ₂ [Mo ₅ O ₁₆]	2-D	34	11	~4	~49	3.21	~0.92	[26]
(C ₈ H ₁₂ N) ₂ [Mo ₅ O ₁₆]	2-D	23	15	~2	~41	1.53	~0.95	[26]
(C ₉ H ₁₄ N) ₂ [Mo ₅ O ₁₆]	2-D	29	15	5	49	1.97	0.91	[42]
(C ₉ H ₁₄ N) ₄ [Mo ₈ O ₂₆]·H ₂ O	0-D	30	18	0	48	1.69	1.00	[42]
(C ₉ H ₁₄ N) ₆ [Mo ₈ O ₂₆ (C ₂ H ₅ O ₂) ₂]	0-D	28	17	0	45	1.66	1.00	[42]

^a Reaction conditions: mole ratio cyclooctane:oxygen = 6.5, air atmosphere (10 bar), 6 h. ^b Conversion (A + B + C) on the basis of oxygen quantity in the reaction mixture.

The molar ratio A/B was slightly higher for **2** (3.15 versus 2.29–2.79 for the remaining IPOMs). The cyclooctane conversions were in the range 46–67%, being lowest for compound **6**, somewhat in parallel to the results verified for olefin epoxidation systems. However, for cyclooctane oxidation, the catalytic results for the remaining IPOMs **1–5** were not considerably different (56–67% cyclooctane conversion at 6 h). More pronounced differences in catalytic results were observed for the epoxidation systems. A comparative study with the literature indicated that **3–5** led to higher cyclooctane conversions than other 0-D, 1-D and 2-D anilinium-type IPOMs tested under similar cyclooctane reaction conditions (Table 7) [26,42]. For all cyclooctane reaction systems in the presence of IPOMs, the ketone product was predominant. The compounds reported in the literature led to 41–50% cyclooctane conversion at 6 h, which is comparable to the results for 2-D **6** (Table 7). The IPOM tetrakis(4-methylanilinium) octamolybdate dihydrate ((C₇H₁₀N)₄[Mo₈O₂₆]·H₂O) was the least active, leading to only 20% conversion [26,42].

3. Materials and Methods

3.1. Materials

For the synthesis of the compounds, MoO₃, acetic acid, HCl and molybdic acid (H₂MoO₄·H₂O (HMO)) were acquired from AVANTOR (Gliwice, Polska) (acs purity). Aniline and anilinium salts (99%) were acquired from Sigma/Aldrich and used as received. For catalytic studies: *cis*-cyclooctene (Cy, 95%, Aldrich, St. Louis, MO, USA), methyl oleate (Ole, 99%, Aldrich), methyl linoleate (LinOle, 95%, Alfa Aesar, Haverhill, MA, USA), α,α,α -trifluorotoluene (TFT, anhydrous, 99.8%, Aldrich), *tert*-butylhydroperoxide (TBHP, 5.5 M in decane, Aldrich), pentane (95%, Carlo Erba, Emmendingen, Germany), 1-butyl-3-methylimidazolium bis(trifluoromethylsulfonyl)imide ([bmim][NtF₂], 99%, Iolitec, Heilbronn, Germany) and acetonitrile (99.9%, Panreac, Heilbronn, Germany) were acquired from commercial sources and used as received.

The syntheses of the new compounds **1**, **2** and **5** are described, and the remaining compounds were synthesized in a similar fashion.

3.2. Synthesis of the IPOM Compounds

Compound 1. Molybdic acid (HMO; 0.01 mol 1.79 g) was added to 150 mL of hot water under reflux. Then, a mixture of 0.01 mol of cyclohexylamine with 50 mL of acetic acid was added and boiled for 0.5 h. After filtering, the filtrate was allowed to crystallize (room temperature). Yield: 85%. Transparent colourless crystals.

Compound 2. Molybdenum oxide (0.01 mol) was added to 15 mL of water and 0.75 mmol of cyclohexylamine. This mixture was kept in an oven for 7 days at 75 °C. Every day, the solution was thoroughly mixed by shaking. The resultant (white coloured)

precipitate was separated by filtration, washed with a water/2-propanol mixture and finally dried in air at room temperature. Yield: *ca.* 100%, white-coloured, fibrillar crystals.

Compound 3. First, 0.01 mol HMO was dissolved in boiling water (150 mL) and then added to a boiling solution mixture of 50 mL acetic acid and 0.01 mol aniline. HCl was added and heated (reflux conditions) for *ca.* 1 h. The solution was left for crystallization. Yield: 92%. The structure of anilinium β -octamolybdate dihydrate was confirmed by XRPD: PDF-4+ card 50-2366.

Compound 4. To a boiling solution of HMO in water (0.01 mol, 150 mL), aniline was added (0.02 mol). This mixture (which became transparent after adding aniline) was heated (reflux conditions) for *ca.* 2 h, and then left for crystallization under ambient conditions. After *ca.* 2–3 months, white-coloured fibrillar crystals were obtained. Yield: *ca.* 60%. Crystallization can be accelerated by nucleation using previously obtained crystals (or even crystallites of compound 5). The structure of anilinium trimolybdate tetrahydrate was confirmed by XRPD: PDF-4+ 49-2407.

Compound 5. To a boiling solution of HMO in water (0.01 mol, 150 mL H₂O), aniline was added (0.02 mol) and kept under reflux for *ca.* 2 h. Then, the solution was cooled down slowly and then kept at *ca.* 80 °C overnight. After *ca.* 12 h, the reaction mixture turned into a white gelatinous product. Microscope observation indicated that fibrillar crystals were formed. Yield: 66%. The structure of anilinium trimolybdate dihydrate was confirmed by XRPD: PDF-4+ card 50-2402.

Compound 6. Molybdic acid (0.01 mol, 1.79 g) was dissolved in 150 mL water under reflux. Then, a solution of 0.0075 mol of anilinium sulphate dissolved in 25 mL water was added and heated (reflux conditions) for 24 h. The obtained precipitate was separated by filtration and dried in air at room temperature. Yield: *ca.* 100%. Very fine, white-greyish-coloured powder. The structure of anilinium pentamolybdate was confirmed by XRPD: PDF-4+ 50-2221.

3.3. Characterisation of the Compounds

X-ray powder/single crystal diffraction. The X-ray powder diffraction (XRPD) investigations were performed for **2** and **5** and single crystal X-ray diffraction (XRD) for **1**. The temperature during measurements was 293(2) K in case of XRPD and 100 K for the single crystal investigations.

The XRPD data were collected using PANalytical X'Pert Pro MPD diffractometer, and single-crystal data using a SuperNova (Oxford Diffraction). High Score software and the PDF-4+ [ICDD, 2022] database were used for the analysis of the XRPD data. Powder diffraction studies were performed using the Expo2014 program [43] to locate Mo and O atoms, and FOX [44] to find the position and orientation of the organic moieties. Finally, restrained Rietveld refinement was performed with the use of Jana2006 [45]. Figures S7 and S8) present Rietveld refinement plots for **2** and **3**, respectively.

Structure solution and refinement of **1** was performed using SHELXS-97 and SHELXL-2013 programs [46]. To find the location of the hydrogen atoms, difference Fourier maps were used. For all non-hydrogen atoms, anisotropic refinement was used.

The Diamond [47] and Mercury [48] programs were used for visualization of the crystal structures of the obtained compounds.

The density D_x each compound was calculated as the ratio of mass/volume (determined by X-ray). For isopolymolybdates, the degree of condensation (DC) equals the ratio of (number of Mo atoms)/(0.5 \times (cluster charge)).

X-ray thermal decomposition. X-ray thermal decomposition patterns were measured using Philips X'Pert Pro MPD. X-ray data for compounds **1**, **2** and **5** was collected at the following temperatures: 25, 50, 75, 100, 125, 150, 175, 200, 225, 250, 300, 350, 400, 450, 500, 550, 600 °C and again at 25 °C. The 2θ range was 5–70°. The heating rate was 5 °C min⁻¹ and the cooling rate was 10 °C min⁻¹.

3.4. Catalytic Tests

3.4.1. Olefin Epoxidation

In this work, the substrates tested for epoxidation reactions were *cis*-cyclooctene (Cy), methyl oleate (Ole) and methyl linoleate (Lin). The catalytic reactions were carried out in 10 mL borosilicate reactors equipped with a Teflon valve (for sampling), at 55 or 70 °C with magnetic stirring, using an amount of catalyst equivalent to 18 µmol of Mo, 1.8 mmol of olefin and 1 mL of α,α,α -trifluorotoluene (TFT). The mixture of catalyst/solvent/olefin was pre-heated at the reaction temperature. Then, the oxidant TBHP (also preheated) was added (2.75 mmol (for Cy) or 5.5 mmol (for Ole and Lin)) to the reaction mixture, and this was taken as the initial instant of the reaction.

The reactions were monitored by gas chromatography, using an Agilent 7820A GC equipped with a DB-5 capillary column (30 m \times 0.25 mm \times 0.25 µm) and an FID detector with H₂ as the carrier gas (for supportive chromatograms please see Figure S18). Quantifications were based on calibrations using undecane (for Cy reactions) or methyl decanoate (for Ole and Lin reactions) as internal standards. The reaction products were identified by GC-MS (Trace GC 2000 Series Thermo Quest CE Instruments GC; Thermo-Scientific DSQ II), using He as the carrier gas. The product identifications were based on commercial mass spectrometry databases (Wiley229, NIST147, NIST107, NIST27, NISTChemistry WebBook, MAINLIB) and mass spectra similarities.

The reaction systems consisted of a biphasic solid–liquid mixture. The homogeneous or heterogeneous nature of the catalytic reaction Cy/TFT/TBHP was studied by carrying out contact tests (ct) as follows: the mixture of catalyst/TFT/TBHP was stirred (1000 rpm) for 1 h at 70 °C, and then cooled to room temperature and passed through a PTFE membrane (0.2 µm pore size) filter. The filtrate was transferred immediately to a separate (empty) reactor, preheated at 70 °C, and subsequently Cy (also preheated) was added in an amount equivalent to that typically used (initial molar ratio Cy:TBHP = 1:1.5). The evolution of the homogeneous phase reaction was monitored by GC as described above. The attempts to precipitate the species from the reaction mixtures involved the addition of solvents such as *n*-pentane, *n*-hexane and acetone, and keeping the solutions at 4 °C, which unfortunately was not sufficient to precipitate measurable amounts of solid.

At the end of Cy reaction, the solids were separated from the reaction mixture by centrifugation (5000 rpm) and thoroughly washed with pentane. The solids were dried overnight under atmospheric conditions, followed by a vacuum drying for 1 h at 60 °C. The recovered solids were used in a second batch run at 70 °C, keeping constant the initial mass ratio of catalyst/olefin/oxidant used in run 1.

3.4.2. Kinetic Modelling

Kinetic models were developed considering perfectly stirred, isothermal batch reactors, and corresponding material balance according to Equation (1):

$$\frac{dC_i}{dt} = r_i \quad (1)$$

where C_i is the molar concentration of species i (M), t is the reaction time (h) and r_i is the reaction rate of species i . The material balances closed in 100% for the substrates Cy (considering CyO), Ole (considering OleOx) and Lin (considering monoepoxides, diepoxides and LinFur). Details of the kinetic models are described in the Supplementary Materials. Three different kinetic models were firstly developed (for Cy epoxidation). The simplest model considered irreversible, first-order reactions for all steps; the second model considered second-order reactions with the oxidant (these two models considered that the epoxidation reaction kinetics was not governed by the rate of formation of active oxidizing species); and the third model considered second-order reactions and the kinetics of formation of active oxidizing species (Mo+TBHP). The three models fitted the experimental data well. Hence, the discussed kinetic models for the Cy, Ole and Lin reactions were based on

the assumptions for the simplest model, e.g., for Cy, the equations 1, 2 and 3 with the rate constant k_{Cy} (h^{-1}):

$$\frac{dC_{Cy}}{dt} = -k_{Cy} C_{Cy} \quad (2)$$

$$\frac{dC_{CyO}}{dt} = k_{Cy} C_{Cy} \quad (3)$$

3.4.3. Cyclooctane Oxidation

The oxidation of cyclooctane was experimentally performed as previously described [26,49,50]. The experiment was carried out in a stainless-steel batch reactor system at 120 °C and under an air pressure of 10 atm. The cyclooctane-to-oxygen molar ratio was 6.5. The reactor was cooled after 6 h, followed by sampling and analytic analysis. The oxidation products cyclooctanone (A) and cyclooctanol (B) were analysed by an Agilent 6890 N Gas Chromatograph (FID detector) equipped with an Innowax (30 m × 0.53 mm × 1.0 μm) column, using an internal standard (chlorobenzene). The amount of suberic acid was determined by the back titration method (the sample is mixed with excess NaOH/KOH and stirred, followed by titration using HCl).

4. Conclusions

The ionic polymolybdate compounds (IPOM) cyclohexylammonium β-octamolybdate dihydrate (1), cyclohexylammonium trimolybdate hydrate (2), anilinium β-octamolybdate dihydrate (3), anilinium trimolybdate tetrahydrate (4) and anilinium trimolybdate dihydrate (5) were synthesized via simple, eco-friendly one-pot routes and studied as epoxidation catalysts of olefins (*cis*-cyclooctene and FAMES) using *tert*-butylhydroperoxide as oxidant. Depending on the IPOM synthesis conditions and the type of molybdenum precursor, IPOM compounds with different structural dimensionality, density D_x and ratio of terminal oxo groups/molybdenum atoms ($n(\text{oxo})/\text{Mo}$) were formed. The different compounds led to different olefin epoxidation reaction kinetics, and no direct structure–activity correlations could be established for all IPOMs. The catalytic studies indicated that the reactions were essentially homogeneous in nature. Accordingly, the (yet unknown) types of soluble metal species may be structurally different, contributing with different intrinsic activities to the overall reaction kinetics.

Nevertheless, the IPOM compounds promoted the epoxidation of biobased fatty acid methyl esters, namely methyl oleate and methyl linoleate, leading to conversions of at least 81% at 4 h, 70 °C, and the corresponding epoxides, as well as furan-type products in the case of the Lin reaction. They also promoted cyclooctane oxidation, although the difference in the catalytic performances of the catalysts seemed less pronounced than for the epoxidation systems. Overall, for the studied substrate scope and reaction scope, 1–5 seemed more active than 6. Insights into the factors influencing the catalytic performances may call for in situ characterization of dissolved metal species involved in the catalytic processes, which is challenging partly due to the complexity of the liquid–solid, multicomponent systems.

Supplementary Materials: The following supporting information can be downloaded at: <https://www.mdpi.com/article/10.3390/catal14040251/s1>, Figure S1: TG/DSC study of cyclohexylammonium β-octamolybdate dihydrate (1). Figure S2: TG/DSC study of cyclohexylammonium trimolybdate hydrate (2). Figure S3: TG/DSC study of anilinium trimolybdate dihydrate (5). Figure S4: XRPD/temp. study of cyclohexylammonium β-octamolybdate dihydrate (1). Figure S5: XRPD/temp study of cyclohexylammonium trimolybdate hydrate (2). Figure S6: XRPD/temp study of anilinium trimolybdate dihydrate (5). Figure S7: Cyclohexylammonium trimolybdate hydrate—Rietveld refinement plots (2). Figure S8: Anilinium trimolybdate dihydrate—Rietveld refinement plots (5). Table S1: Cyclohexylammonium β-octamolybdate dihydrate—interatomic distances (1). Table S2: Cyclohexylammonium trimolybdate hydrate—interatomic distances (2). Table S3: Anilinium trimolybdate dihydrate—interatomic distances (5). Figure S9: Experimental data (markers) and calculated kinetic curves (lines) for Cy (o) and epoxide CyO (Δ) concentration, based on the model A, for catalyst 1 (a), 2 (b), 3 (c), 4 (d), 5 (e) and 6 (f), at 70 °C. Figure S10: Experimental data

(markers) and calculated kinetic curves (lines) for Cy (o) and epoxide CyO (Δ) concentration, based on the model B, for catalyst 1 (a), 2 (b), 3 (c), 4 (d), 5 (e) and 6 (f), at 70 °C. Figure S11: Experimental data (markers) and calculated kinetic curves (lines) for Cy (o) and epoxide CyO (Δ) concentration, based on the model C, for catalyst 1 (a), 2 (b), 3 (c), 4 (d), 5 (e) and 6 (f), at 70 °C. Table S4: Calculated data based on kinetic models A and B, for the Cy reaction, at 70 °C. Table S5: Calculated data based on kinetic model C, for the Cy reaction, at 70 °C. Scheme S2: Mechanistic proposal for the reaction of the olefins, considering irreversible, first-order reactions (same as Scheme 1 of the main text, serves as guide). Figure S12: Experimental data (markers) and calculated kinetic curves (lines) for Ole (o) and OleOx (Δ) concentration for catalyst 1 (a), 2 (b), 3 (c), 4 (d), 5 (e) and 6 (f), at 70 °C. Figure S13: Experimental data (markers) and calculated kinetic curves (lines) for Lin (o), LinOx (Δ), LimDiOx (\times) and LinFur (+) concentration for catalyst 1 (a), 2 (b), 3 (c), 4 (d), 5 (e) and 6 (f), at 70 °C. Figure S14: cis-Cyclooctene epoxidation with TBHP, in the presence of the IPOM catalysts 3–5, at 55 °C. Epoxide selectivity was always 100 %. Table S6: Comparison of the catalytic results for 3–5 to literature data for IPOM compounds possessing anilinium derivatives as organic components, tested for the Cy/TBHP reaction, at 55 °C. Figure S15: Typical epoxidation catalytic test (with catalyst) (o) and contact tests (\times) for cis-cyclooctene epoxidation with TBHP, in the presence of the IPOM catalysts 1–6, at 70 °C. Figure S16: ATR FT-IR spectra (a) and powder XRD patterns (b) of the original and recovered solids 1, 2, 3 and 5. The experimental details of the characterisation techniques are indicated. Figure S17: Kinetic constants as a function of density D_x (left) and $n(\text{oxo})/\text{Mo}$ ratio (right), for the Cy6N (a, b) and Anil (c, d) families of IPOM catalysts with different substrates (Cy (circles), Ole (squares) and Lin (triangles); the dotted lines are trendlines). Figure S18: Examples of chromatograms for Cy, Ole and Lin reactions.

Author Contributions: Conceptualization, W.L. and A.A.V.; validation, P.N. (epoxidation), G.S. (kinetic modelling), B.D.N. (crystalline phase analysis, TG/DSC analyses), K.P. (cyclooctane oxidation), P.S. (single crystal), A.A.V. (epoxidation) and W.L. (XRPD); investigation, P.N., G.S., B.D.N., K.P. and P.S.; resources, W.L. and A.A.V.; writing—original draft preparation, P.N.; writing—review and editing, A.A.V. and W.L.; visualization, P.N., W.L. and A.A.V.; supervision, P.N., W.L. and A.A.V.; project administration, W.L. and A.A.V.; funding acquisition, W.L. and A.A.V. All authors have read and agreed to the published version of the manuscript.

Funding: This work was developed within the scope of the project CICECO-Aveiro Institute of Materials, UIDB/50011/2020, UIDP/50011/2020, and LA/P/0006/2020, financed by national funds through the FCT/MCTES (PIDDAC). The study (at Jagiellonian University) was carried out using research infrastructure purchased with the funds of the European Union in the framework of the Smart Growth Operational Programme, Measure 4.2; Grant No. POIR.04.02.00-00-D001/20, ATOMIN 2.0—ATOMic scale science for the INnovative economy.

Data Availability Statement: Data is essentially contained within the article or Supplementary Materials.

Acknowledgments: The authors are grateful to the mentioned funders.

Conflicts of Interest: The authors declare no conflicts of interest. The funders had no role in the design of the study; in the collection, analyses, or interpretation of data; in the writing of the manuscript; or in the decision to publish the results.

References

1. Lligadas, G.; Ronda, J.C.; Galià, M.; Biermann, U.; Metzger, J.O. Synthesis and Characterization of Polyurethanes from Epoxidized Methyl Oleate Based Polyether Polyols as Renewable Resources. *J. Polym. Sci. A Polym. Chem.* **2006**, *44*, 634–645. [[CrossRef](#)]
2. Musik, M.; Janus, E.; Pelech, R.; Sałaciński, Ł. Effective Epoxidation of Fatty Acid Methyl Esters with Hydrogen Peroxide by the Catalytic System $\text{H}_3\text{PW}_{12}\text{O}_{40}$ /Quaternary Phosphonium Salts. *Catalysts* **2021**, *11*, 1058. [[CrossRef](#)]
3. Hájek, M.; Hájek, T.; Kocián, D.; Frolich, K.; Peller, A. Epoxidation of Methyl Esters as Valuable Biomolecules: Monitoring of Reaction. *Molecules* **2023**, *28*, 2819. [[CrossRef](#)]
4. Sharma, B.K.; Doll, M.; Erhan, S.Z. Oxidation, Friction Reducing, and Low Temperature Properties of Epoxy Fatty Acid Methyl Esters. *Green Chem.* **2007**, *9*, 469–474. [[CrossRef](#)]
5. Wadumesthrige, K.; Salley, S.O.; Ng, K.Y.S. Effects of Partial Hydrogenation, Epoxidation, and Hydroxylation on the Fuel Properties of Fatty Acid Methyl Esters. *Eur. J. Lipid Sci. Technol.* **2009**, *90*, 1292–1299. [[CrossRef](#)]
6. Available online: <https://polymer-additives.specialchem.com/selectors/tr-vikoflex> (accessed on 21 December 2023).
7. Turco, R.; Tesser, R.; Russo, V.; Vitiello, R.; Fagnano, M.; Di Serio, M. Comparison of Different Possible Technologies for Epoxidation of Cynara Cardunculus Seed Oil. *Eur. J. Lipid Sci. Technol.* **2020**, *122*, 1900100. [[CrossRef](#)]

8. Available online: <https://www.fortunebusinessinsights.com/epoxidized-soybean-oil-market-104343> (accessed on 21 December 2023).
9. Meng, Y.; Taddeo, F.; Aguilera, A.F.; Cai, X.; Russo, V.; Tolvanen, P.; Leveneur, S. The Lord of the Chemical Rings: Catalytic Synthesis of Important Industrial Epoxide Compounds. *Catalysts* **2021**, *11*, 765. [CrossRef]
10. Yan, W.; Wang, Z.; Luo, C.; Xia, X.; Liu, Z.; Zhao, Y.; Du, F.; Jin, X. Opportunities and Emerging Challenges of the Heterogeneous Metal-Based Catalysts for Vegetable Oil Epoxidation. *ACS Sustain. Chem. Eng.* **2022**, *10*, 7426–7446. [CrossRef]
11. Cucciolo, M.E.; Di Serio, M.; Esposito, R.; Melchiorre, M.; Ruffo, F.; Russo, V.; Tesser, R.; Turco, R.; Vitiello, R. Catalysis for Oleochemical Platforms. *Eur. J. Inorg. Chem.* **2023**, *26*, e202200783. [CrossRef]
12. Pinaeva, L.G.; Noskov, A.S. Prospects for the Development of Catalysts for the Oxidation Processes of Advanced Propylene Processing. *Catal. Ind.* **2020**, *12*, 176–200. [CrossRef]
13. Shen, Y.; Jiang, P.; Wai, P.T.; Gu, Q.; Zhang, W. Recent Progress in Application of Molybdenum-Based Catalysts for Epoxidation of Alkenes. *Catalysts* **2019**, *9*, 31. [CrossRef]
14. Brégeault, J.M. Transition-Metal Complexes for Liquid-Phase Catalytic Oxidation: Some Aspects of Industrial Reactions and of Emerging Technologies. *J. Chem. Soc. Dalton Trans.* **2003**, *3*, 3289–3302. [CrossRef]
15. Pisk, J.; Agustin, D. Molybdenum, Vanadium, and Tungsten-Based Catalysts for Sustainable (Ep)Oxidation. *Molecules* **2022**, *27*, 6011. [CrossRef]
16. Bridgeman, A.J.; Cavigliasso, G. Electronic Structure of the α and β Isomers of $[\text{Mo}_8\text{O}_{26}]^{4-}$. *Inorg. Chem.* **2002**, *41*, 3500–3507. [CrossRef]
17. Available online: https://colapret.cm.utexas.edu/courses/320M%20Syllabus_Sp2019.pdf (accessed on 21 December 2023).
18. Available online: <https://openstax.org/books/organic-chemistry/pages/24-4-basicity-of-arylamines?query=cyclohexylammonium> (accessed on 21 December 2023).
19. Božek, B.; Neves, P.; Valente, A.A. Ionic Ammonium and Anilinium Based Polymolybdate Hybrid Catalysts for Olefin Epoxidation. *Appl. Catal. A Gen.* **2018**, *564*, 13–25. [CrossRef]
20. Zhou, M.-D.; Liu, M.-J.; Huang, L.-L.; Zhang, J.; Wang, J.-Y.; Li, X.-B.; Kühn, F.E.; Zang, S.-L. Olefin Epoxidation with Hydrogen Peroxide Using Octamolybdate-Based Self-Separating Catalysts. *Green Chem.* **2015**, *17*, 1186–1193. [CrossRef]
21. Kumar, A.; Gupta, A.K.; Devi, M.; Gonsalves, K.E.; Pradeep, C.P. Engineering Multifunctionality in Hybrid Polyoxometalates: Aromatic Sulfonium Octamolybdates as Excellent Photochromic Materials and Self-Separating Catalysts for Epoxidation. *Inorg. Chem.* **2017**, *56*, 10325–10336. [CrossRef]
22. Neves, P.; Amarante, T.R.; Valente, A.A.; Pillinger, M.; Gonçalves, I.S. Catalytic Application of an Octamolybdate Salt (H_3biim) $_4$ $[\beta\text{-Mo}_8\text{O}_{26}]$ in Olefin Epoxidation ($\text{H}_2\text{biim} = 2,2'$ -Biimidazole). *Catal. Lett.* **2016**, *146*, 841–850. [CrossRef]
23. Gamelas, C.A.; Neves, P.; Gomes, A.C.; Valente, A.A.; Romão, C.C.; Gonçalves, I.S.; Pillinger, M. Molybdenum(II) Diiodo-Tricarbonyl Complexes Containing Nitrogen Donor Ligands as Catalyst Precursors for the Epoxidation of Methyl Oleate. *Catal. Lett.* **2012**, *142*, 1218–1224. [CrossRef]
24. Available online: <https://www.masterorganicchemistry.com/2017/04/18/basicity-of-amines-and-pknh/> (accessed on 21 December 2023).
25. Kama, A.B.; Dessapt, R.; Serier-Brault, H.; Sidibe, M.; Diop, C.A.K.; Gautier, R. Stabilization of β -Octamolybdate with Large Counterions. *J. Mol. Struct.* **2017**, *1141*, 698–702. [CrossRef]
26. Szyman, A.; Pamin, K.; Połtowicz, J. Molybdenum Complexes as Catalysts for the Oxidation of Cycloalkanes with Molecular Oxygen. *Catal. Lett.* **2016**, *146*, 998–1010. [CrossRef]
27. Veiros, L.F.; Prazeres, A.; Costa, P.J.; Romão, C.C.; Kühn, F.E.; José Calhorda, M. Olefin Epoxidation with Tert-Butyl Hydroperoxide Catalyzed by $\text{MoO}_2\text{X}_2\text{L}$ Complexes: A DFT Mechanistic Study. *Dalton Trans.* **2006**, *11*, 1383–1389. [CrossRef] [PubMed]
28. Comas-Vives, A.; Lledós, A.; Poli, R. A Computational Study of the Olefin Epoxidation Mechanism Catalyzed by Cyclopentadienylloxidomolybdenum(VI) Complexes. *Chem. Eur. J.* **2010**, *16*, 2147–2158. [CrossRef] [PubMed]
29. Al-Ajlouni, A.; Valerie, A.A.; Nunes, C.D.; Pillinger, M.; Santos, A.M.; Zhao, J.; Romão, C.C.; Gonçalves, I.S.; Kühn, F.E. Kinetics of Cyclooctene Epoxidation with tert-Butyl Hydroperoxide in the Presence of $[\text{MoO}_2\text{X}_2\text{L}]$ -Type Catalysts (L = Bidentate Lewis Base). *Eur. J. Inorg. Chem.* **2005**, *2005*, 1716–1723. [CrossRef]
30. Prazeres, A.; Santos, A.M.; Calhorda, M.J.; Roma, C.C.; Gonçalves, I.S. Octahedral Bipyridine and Bipyrimidine Dioxomolybdenum (VI) Complexes. *Chem. Eur. J.* **2002**, *8*, 2370–2383. [CrossRef]
31. Garrido, G.; Rosés, M.; Ràfols, C.; Bosch, E. Acidity of Several Anilinium Derivatives in Pure Tetrahydrofuran. *J. Solut. Chem.* **2008**, *37*, 689–700. [CrossRef]
32. Neves, P.; Gomes, A.C.; Cunha-Silva, L.; Valente, A.A.; Pillinger, M.; Gonçalves, I.S. Silicododecamolybdate/Pyridinium-Tetrazole Hybrid Molecular Salt as a Catalyst for the Epoxidation of Bio-Derived Olefins. *Inorg. Chim. Acta A* **2021**, *516*, 120129. [CrossRef]
33. Nunes, M.S.; Gomes, A.C.; Neves, P.; Mendes, R.F.; Almeida Paz, F.A.; Lopes, A.D.; Pillinger, M.; Gonçalves, I.S.; Valente, A.A. Molybdenum(VI) Complexes with Ligands Derived from 5-(2-Pyridyl)-2H-Tetrazole as Catalysts for the Epoxidation of Olefins. *Catal. Today* **2023**, *423*, 114273. [CrossRef]
34. Herman, K.; Foodtechn, J. Catalytic Epoxidation of Methyl Linoleate-Cyclisation Products of Epoxyacid Esters. *Fat. Sci. Technol.* **1995**, *97*, 269–273.
35. Dorado, V.; Herrerías, C.I.; Fraile, J.M. Catalytic Hydrolysis of Epoxyfatty Esters with Solid Sulfonic Acids. *Mol. Catal.* **2023**, *547*, 113282. [CrossRef]

36. Piazza, G.J.; Nuñez, A.; Foglia, T.A. Hydrolysis of Mono- and Diepoxyoctadecanoates by Alumina. *J. Am. Oil Chem. Soc.* **2003**, *80*, 901–904. [CrossRef]
37. Bantchev, G.B.; Doll, K.M.; Biresaw, G.; Vermillion, K.E. Formation of Furan Fatty Alkyl Esters from Their Bis-Epoxy Fatty Esters. *J. Am. Oil Chem. Soc.* **2014**, *91*, 2117–2123. [CrossRef]
38. Stolp, L.J.; Joseph, E.; Kodali, D.R. Synthesis and Evaluation of Soy Fatty Acid Ester Estolides as Bioplasticizers in Poly(Vinyl Chloride). *J. Am. Oil Chem. Soc.* **2019**, *96*, 1291–1302. [CrossRef]
39. Wolfe, J.P.; Hay, M.B. Recent Advances in the Stereoselective Synthesis of Tetrahydrofurans. *Tetrahedron* **2007**, *63*, 261–290. [CrossRef] [PubMed]
40. Capon, R.J.; Barrow, R.A. Acid-Mediated Conversion of Methylene-Interrupted Bisepoxides to Tetrahydrofurans: A Biomimetic Transformation. *J. Org. Chem.* **1998**, *63*, 75–83. [CrossRef] [PubMed]
41. Araj, N.; Chatel, G.; Moores, A.; Jérôme, F.; De Oliveira Vigier, K. Oxidative Cyclization of Linoleic Acid in the Presence of Hydrogen Peroxide and Phosphotungstic Acid. *Mol. Catal.* **2020**, *493*, 111084. [CrossRef]
42. Oszajca, M.; Nitek, W.; Rafalska-Łasocha, A.; Pamin, K.; Połtowicz, J.; Łasocha, W. Synthesis, Crystal Structure and Selected Properties of Three New 4-Propylanilinium Polyoxomolybdates. *J. Mol. Struct.* **2023**, *1273*, 134292. [CrossRef]
43. Altomare, A.; Cuocci, C.; Giovacazzo, C.; Moliterni, A.; Rizzi, R.; Corriero, N.; Falcicchio, A. EXPO2013: A Kit of Tools for Phasing Crystal Structures from Powder Data. *J. Appl. Crystallogr.* **2013**, *46*, 1231–1235. [CrossRef]
44. Favre-Nicolin, V.; Cerný, R. FOX, 'free Objects for Crystallography': A Modular Approach to Ab Initio Structure Determination from Powder Diffraction. *J. Appl. Crystallogr.* **2002**, *35*, 734–743. [CrossRef]
45. Petricek, V.; Dusek, M.; Palatinus, L. *The Crystallographic Computing System*; Institute of Physics: Jana, Czech Republic, 2006.
46. Sheldrick, G.M. A Short History of SHELX. *Acta Crystallogr. A* **2008**, *64*, 112–122. [CrossRef]
47. Brandenburg, K. Diamond Version 3.2g, Crystal Impact GbR, Bonn, Germany, 1997–2001. Available online: <http://www.crystalimpact.com/diamond> (accessed on 4 January 2023).
48. Macrae, C.F.; Edgington, P.R.; McCabe, P.; Pidcock, E.; Shields, G.P.; Taylor, R.; Towler, M.; Van De Streek, J. Mercury: Visualization and Analysis of Crystal Structures. *J. Appl. Crystallogr.* **2006**, *39*, 453–457. [CrossRef]
49. Božek, B.; Neves, P.; Oszajca, M.; Valente, A.A.; Połtowicz, J.; Pamin, K.; Łasocha, W. Simple Hybrids Based on Mo or W Oxides and Diamines: Structure Determination and Catalytic Properties. *Catal. Lett.* **2020**, *150*, 713–727. [CrossRef]
50. Pamin, K.; Jachimska, B.; Onik, K.; Połtowicz, J.; Grabowski, R. Electrostatic Self-Assembly of Polyoxometalates on Chitosan as Catalysts of Oxidation of Cyclic Hydrocarbons. *Catal. Lett.* **2009**, *127*, 167–174. [CrossRef]

Disclaimer/Publisher's Note: The statements, opinions and data contained in all publications are solely those of the individual author(s) and contributor(s) and not of MDPI and/or the editor(s). MDPI and/or the editor(s) disclaim responsibility for any injury to people or property resulting from any ideas, methods, instructions or products referred to in the content.